Nanoscale

RSC Publishing

PAPER

View Article Online
View Journal | View Issue

Cite this: *Nanoscale*, 2013, **5**, 6812

Atomistic nucleation sites of Pt nanoparticles on N-doped carbon nanotubes†

Chia-Liang Sun,*[a] Chih-Wen Pao,[b] Huang-Ming Tsai,[b] Jau-Wern Chiou,[c] Sekhar C. Ray,*[d] Houng-Wei Wang,[e] Michitoshi Hayashi,[e] Li-Chyong Chen,[e] Hong-Ji Lin,[b] Jyh-Fu Lee,[b] Li Chang,[f] Min-Hsiung Tsai,[g] Kuei-Hsien Chen[h] and Way-Faung Pong*[i]

Received 11th March 2013
Accepted 16th May 2013

DOI: 10.1039/c3nr01234d

www.rsc.org/nanoscale

The atomistic nucleation sites of Pt nanoparticles (Pt NPs) on N-doped carbon nanotubes (N-CNTs) were investigated using C and N K-edge and Pt L_3-edge X-ray absorption near-edge structure (XANES)/extended X-ray absorption fine structure (EXAFS) spectroscopy. Transmission electron microscopy and XANES/EXAFS results revealed that the self-organized Pt NPs on N-CNTs are uniformly distributed because of the relatively high binding energies of the adsorbed Pt atoms at the imperfect sites. During the atomistic nucleation process of Pt NPs on N-CNTs, stable Pt–C and Pt–N bonds are presumably formed, and charge transfer occurs at the surface/interface of the N-CNTs. The findings in this study were consistent with density functional theory calculations performed using cluster models for the undoped, substitutional-N-doped and pyridine-like-N-doped CNTs.

Introduction

Organized nanoparticles (NPs) are interesting from both fundamental and practical points of view.[1–8] Researchers have loaded NPs onto support materials to influence their properties and structures for catalytic applications.[9–16] NPs with sizes of 2–6 nm are preferred to nanostructured composites because they have a larger surface-area-to-volume ratio. Among the numerous NP catalysts, Pt NPs have been extensively used for catalytic reactions in fuel cells because Pt that is loaded onto nanostructured composites[17–20] results in a very high conversion efficiency and high electrochemical stability. The catalytic activity and efficiency of Pt NPs should be increased to reduce the operational costs of proton exchange membrane fuel cells and related applications. The layered structure of the catalyst can be modified for this purpose. The performance of Pt catalysts has been observed to vary greatly with the structure of the underlying carbon substrate during the operation of a fuel cell. In addition, Pt NPs cast onto carbon nanotubes (CNTs) or onto nanotubule membranes have been extensively used to prepare Pt catalysts for such applications.[12,21]

Recently, we have reviewed the electronic, optical and electrochemical properties along with the electronic behaviors of nitrogen-substituted single-walled carbon nanotubes (SWCNTs); these behaviors underlie density functional theory (DFT) simulations.[22] In our previous study,[23] we investigated the atomic-scale deformation of nitrogen-doped carbon nanotubes (N-CNTs). In that investigation, the deformed structures were observed to be associated with the concentration of N dopants with a pyridine-like structure. DFT calculations showed that the homogeneously distributed isolated N dopants in the form of substitutional-N clusters enlarge the diameter of the CNTs. In the present study, we investigate the synthesis of well-dispersed Pt NPs on aligned N-CNTs by a plasma-based vapor deposition technique that is based on atomic-scale metal–support interactions.[24,25] The bonding of arrayed nanomaterials has been characterized by transmission electron microscopy (TEM). The TEM images revealed that the surface of the N-CNT nanostructures could be modified through doping, which is critical for forming Pt NPs. The TEM results are consistent with the C and N K-edge and the Pt L_3-edge X-ray absorption near-edge structure (XANES)/extended X-ray absorption fine structure (EXAFS) spectroscopy results, which indicate that Pt NPs are uniformly dispersed on the N-CNTs (N-CNTs:Pt) and that stable Pt–C and Pt–N bonds are

[a]*Department of Chemical and Materials Engineering, Chang Gung University, Kwei-Shan, Tao-Yuan 333, Taiwan. E-mail: sunchialiang@gmail.com*

[b]*National Synchrotron Radiation Research Center, Hsinchu 300, Taiwan*

[c]*Department of Applied Physics, National University of Kaohsiung, Kaohsiung 811, Taiwan*

[d]*School of Physics, DST/NRF Centre of Excellence in Strong Materials and Materials Physics Research Institute (MPRI), University of the Witwatersrand, P/Bag 3, WITS 2050, Johannesburg, South Africa. E-mail: Sekhar.Ray@wits.ac.za*

[e]*Center for Condensed Matter Sciences, National Taiwan University, Taipei 106, Taiwan*

[f]*Department of Materials Science and Engineering, National Chiao Tung University, Hsinchu 300, Taiwan*

[g]*Department of Physics, National Sun Yat-Sen University, Kaohsiung 811, Taiwan*

[h]*Institute of Atomic and Molecular Sciences, Academia Sinica, Taipei 106, Taiwan*

[i]*Department of Physics, Tamkang University, Tamsui 251, Taiwan. E-mail: wfpong@mail.tku.edu.tw*

† Electronic supplementary information (ESI). See: DOI: 10.1039/c3nr01234d

presumably formed at the surface/interface of the N-CNTs. We performed DFT calculations of the binding energy between the Pt atoms and the surface of the N-CNTs[26,27] and found a large difference in the binding energy between the perfect and doping sites, which is related to the trapping of clusters on the tube surface.[6] A combination of experimental measurements and DFT calculations can elucidate the atom-by-atom construction of nanostructured composites.[28] Such engineered nanocomposite-structured N-CNT:Pt materials are very useful in a variety of applications, which include fuel cells,[29–32] the formation of nanowires from nanotubes,[33] and high-performance electrodes in rechargeable batteries.[34,35]

Experimental

Experimental section and the computation method

Aligned N-doped CNTs were synthesized by the microwave-plasma-enhanced chemical vapour deposition (MPECVD) method. MPECVD growth was performed at a microwave power of 2 kW with a mixture of CH_4, N_2 and H_2 as the source gas and at a substrate temperature of 1000 °C. To deposit Pt NPs, we performed DC sputtering in flowing Ar gas at room temperature, and the deposition time was 15 min. For this sputtering process, the background and sputtering pressures were 5 Pa and 40 Pa, respectively. The sputtering current was 10 mA under a discharge voltage of approximately 100 to 150 volts. The C and N K-edge and the Pt L_3-edge XANES/EXAFS spectroscopies were performed using a high-energy spherical grating monochromator and wiggler beamlines located at NSRRC, Hsinchu, Taiwan. The XANES spectra shown in the figures have been divided by the incident intensity I_0 and normalized to have the same area in the energy range of 315 to 320 eV (430–450 eV) for the C (N) K-edge. The Pt L_3-edge XANES was normalized to the edge-step, $\Delta\mu$, which differs from the value that was extrapolated through simple fitting of the L_3-edge region between 150 and 400 eV and the pre-edge region following the standard procedure for background subtraction. The deposited materials were scratched from the substrate and then dispersed onto a lacey carbon-covered Cu grid for high-resolution TEM observation with electron energy-loss spectroscopy (EELS). In this study, we performed the theoretical simulations using cluster structural models with a DFT calculation level to understand the experimental observations. Three types of CNT cluster models were chosen for Pt-atom binding: (i) $C_{100}H_{20}$, (ii) substitutional-N-doped (sN-doped) $C_{94}N_6H_{20}$ and (iii) pyridine-like N-doped (PyN-doped) $C_{92}N_6H_{20}$ (10,0) clusters. Geometrical structure optimization of these models was fully realized at the B3LYP/6-31G* calculation level and the basis set for the Pt atom was LanL2DZ with effective core potential. The charge distributions and binding energies were generated at the same DFT level. All calculations were performed using the Gaussian 03 software package.[36]

Results and discussion

Fig. 1(a) and (b) present a typical bright-field TEM image and the corresponding electron energy-loss spectroscopy (EELS) map of nitrogen energy-filtered TEM (N-EFTEM) images of the original CNTs, which exhibit a bamboo-like structure.[23,30] The bright part in Fig. 1(b) indicates that the distribution of N in these CNTs is narrower than the diameter of the tube shown in Fig. 1(a). The concentration of N within the CNTs exceeds that in the outer graphite layers. The N atoms in CNTs can substitute at the C sites to form the substitutional and pyridine-like N-sites. The pyridine-like N-sites can cause a positive curvature in CNTs and are responsible for the relatively N-rich linking components.[23] Following Pt-coating, many dark spots with an average diameter of 2 nm are observed on the tube wall (Fig. 1(c)). These dark spots are Pt NPs and are distributed uniformly on the tube wall, as verified by the selected-area electron diffraction pattern and the high-resolution images presented in a previous study.[31] The N-EFTEM map of a single coated nanotube shows a substantially smaller bright area, as

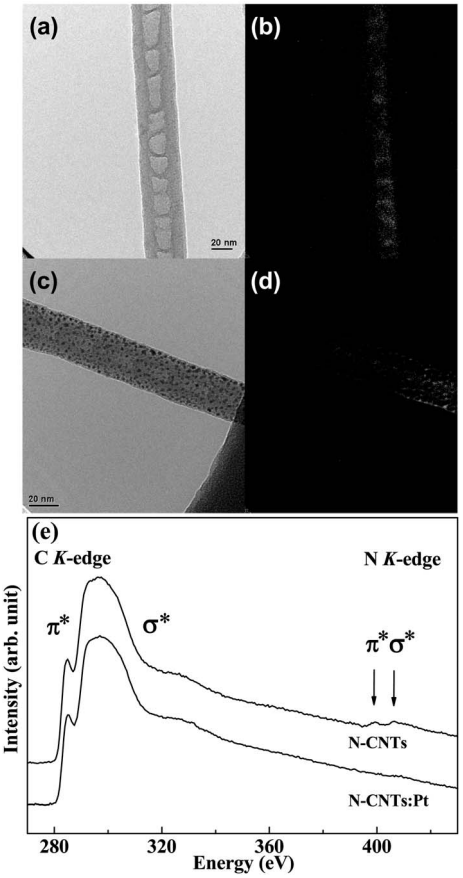

Fig. 1 Visualization of the change in the N signal upon the formation of Pt NPs. (a) and (b) TEM and the corresponding N-EFTEM images of a single N-doped CNT. These images reveal that the interlinked parts of this bamboo-like N-doped CNT contain higher N concentrations. The concentrated N content results in a positive graphene curvature and, therefore, results in the formation of the interlinked parts. (c) and (d) TEM and the corresponding N-EFTEM maps of one Pt-coated N-doped CNT, on the walls of which Pt NPs with a narrow size distribution are well dispersed. These images indicate that the Pt coating weakens the N signal from the nanotube and thereby suggest that the Pt particles selectively bind to the surface N sites. (e) The corresponding EELS spectra of single N-CNTs and Pt-coated N-CNTs. Dramatic weakening of the N K-edge XANES signal in the spectra is consistent with the other images in this figure.

presented in Fig. 1(d). Notably, the full-width at half-maximum of the Pt(111) peak in the X-ray diffraction patterns remains approximately constant as the deposition time is increased,[31] which indicates that the Pt clusters remain at several nucleation sites along their diffusion path rather than coalescing to become larger clusters at few nucleation sites. Fig. 1(e) presents the EELS spectra of an individual N-CNT and an individual N-CNT:Pt. The C K-edge is composed of a step at ~293 eV, which is due to transitions from the C 1s core level to the σ* states, and a peak at ~285 eV, which is due to transitions to the π* states of sp^2 bonds. The N K-edge appears at approximately ~399 eV and 406 eV, which corresponds to π* and σ* features, respectively.[37] Clearly, the Pt coating markedly diminished the intensity of the N signal, whereas the line-shape/intensity of the C K-edge feature was similar to that of the uncoated nanotube. In the N K-edge spectrum, the π* feature is almost invisible and the σ* feature is very weak, which implies that the Pt NPs coated onto the N-CNT surface drastically affected the formation of N bonds.

Fig. 2(a) and (b) display the C and N K-edge XANES spectra, respectively, of the amorphous carbon nitride (a-CN_x) film, the N-CNTs and the N-CNTs:Pt. In the C K-edge XANES spectra of a-CN_x, two features at ~283.2 eV and 286.4 eV are observed in the π* region, and these features are attributed to the C═C- and C═N-bonded pyridine structure; the features at ~291 eV and 295 eV in the σ* region are assigned to the C═C and C–N/C═N bond structures,[38,39] respectively. The π* feature at the C K-edge of the N-CNTs and the N-CNTs:Pt shifted from ~284.1 eV (N-CNTs) to 283.7 eV (N-CNTs:Pt) (as indicated by the dashed lines). Importantly, the intensity of the π* feature of N-CNTs:Pt is substantially lower than that of N-CNTs, which suggests that the Pt–C bond has been formed and that the C atoms most likely acquire electrons from Pt NPs, which, consequently, results in a decrease in the number of C $2p_\pi$ unoccupied states. The feature observed between π* and σ* (in the range 287–288 eV), which is attributable to the mixed states of C═O/C–OH/C–O and other groups,[40,41] is enhanced in the spectrum of N-CNTs:Pt, and this enhancement indicates that Pt NPs strongly modified the surface of N-CNTs. In the σ* region, a plateau-like-feature appeared in the range of 292–308 eV in the spectrum of the N-CNTs. In contrast, the spectral features of the N-CNTs:Pt include a triangular line shape when Pt is coated onto N-CNTs. The modified line shape and the enhanced intensity of the feature in the σ* region of the N-CNTs:Pt may be caused by modification of the C bonding states, deformation of the surface lattice of the N-CNTs during sputtering,[42] and/or the possible formation of new Pt nanocomposites. In the N K-edge XANES spectra presented in Fig. 2(b), the broad features in the spectra of a-CN_x in the ranges of 400–406 eV and 409–430 eV are associated with N 1s → π* and 1s → σ* transitions, respectively, which are superpositions of features of graphite-like and pyridine-like N structures.[23,43] The two well-resolved resonance features at ~402.5 and 403.5 eV in the spectra of N-CNTs are associated with the intercalation and incorporation of N_2 molecules.[38,39,44] The Pt coating significantly reduces the intensities of these two strong features and slightly shifts their positions from ~402.5 eV to 403.0 eV (as indicated by the dashed line). The reduced intensities of these features also suggest the possible formation of new Pt–N bonding states, which involve electron transfer between Pt and N (similar to the case of the Pt–C bonds) on the surface/interface of N-CNTs:Pt and/or the diffusion of N_2 molecules out of the surface of the N-CNTs by local heating during sputtering.[44] The observable feature centered at ~410 eV in the spectra of both N-CNTs and N-CNTs:Pt further supports the presence of graphite-like and pyridine-like N structures.[38,39,44,45] However, the two fine features in the spectrum of N-CNTs at ~417 eV and 421 eV (indicated by two arrows), which were attributed to C═N and C≡N in the σ* region,[46,47] disappeared when the N-CNTs were coated with Pt NPs. The diminished intensity and the shift in the position of the π* features at both the C and the N K-edges indicate the formation of new bonding states in N-CNTs:Pt that were absent in N-CNTs. This finding suggests that, during the sputtering process, clusters of Pt NPs were trapped at both substitutional and pyridine-like N sites rather than on the perfect surface. Thus, we propose that N sites on the surface of CNTs are the preferred nucleation sites for energetic Pt clusters during the sputtering process. Notably, the intensities of the π* features in the spectra of both the C and the N K-edges are significantly reduced upon being decorated with Pt NPs, which strongly indicates the formation of new Pt–C and Pt–N bonds,

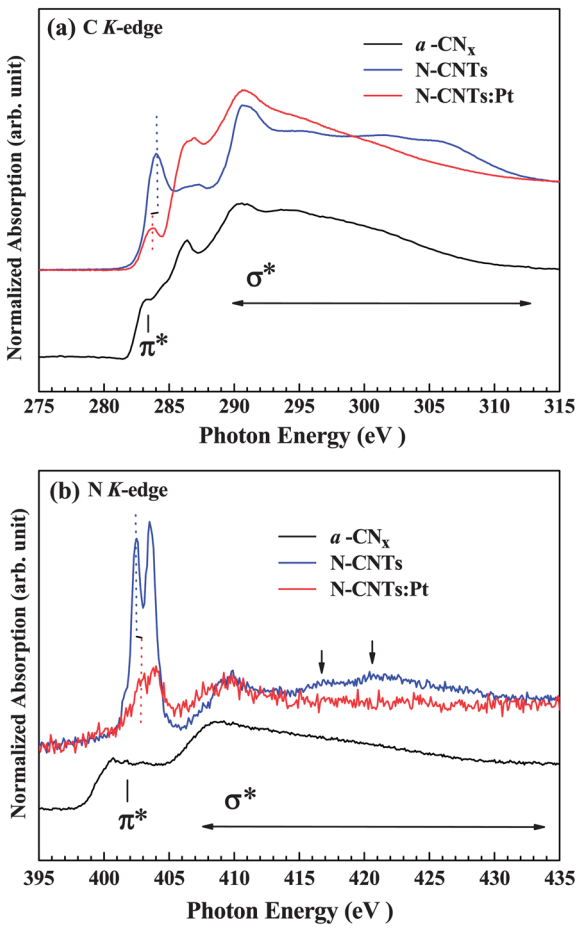

Fig. 2 (a) C K-edge XANES spectra of a-CN_x, N-CNTs and N-CNTs:Pt. (b) N K-edge XANES spectra of a-CN_x, N-CNTs and N-CNTs:Pt.

respectively, and the transfer of electrons between Pt NPs and C and N atoms on the surface/interface of the N-CNTs:Pt.

Fig. 3(a) shows the normalized XANES spectra at the Pt L_3-edge of the N-CNTs:Pt; the spectrum of Pt foil was used as a reference to confirm the transfer of electrons between the Pt NPs and C and N atoms with stable Pt–C and Pt–N bonds in N-CNTs:Pt. The Pt L_3-edge white line (WL) was used to probe the Pt 5d states by exploiting the dipole transition ($2p_{3/2} \rightarrow 5d$).[48–52] The spectrum of the Pt foil exhibits a sharp feature (A) at the edge that is associated with its unfilled 5d orbitals. The general spectral line shape of the N-CNTs:Pt resembles that of the Pt foil, which suggests that the Pt NPs deposited on the N-CNTs still have a face-centered cubic (fcc) structure. A close examination of the WL intensity after the background (indicated by a dashed line) has been subtracted reveals that the intensity of feature A in the spectrum of the N-CNTs:Pt slightly exceeds that in the spectrum of the N-CNTs, as shown in the lower inset of the figure. This comparison clearly suggests that the formation of Pt NPs and their interaction with N-CNTs slightly increase the density of Pt 5d holes.[51] Adora *et al.* performed an X-ray absorption study and clearly showed that, during the chemical reduction of Pt on a carbon support, nucleation and growth of metallic NPs proceed simultaneously.[53] In the present study, the

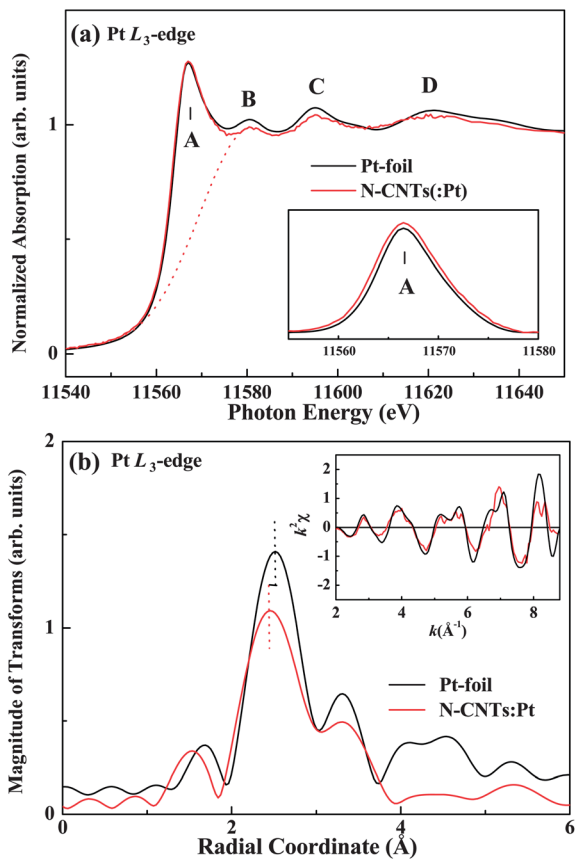

Fig. 3 (a) Pt L_3-edge XANES spectra of N-CNTs:Pt and Pt foil. (b) Fourier-transform spectra from $k = 3$ to 9 Å^{-1} and the corresponding EXAFS oscillation, $k^2\chi(k)$. The inset in (a) shows a plot of the WL feature at the Pt L_3-edge of N-CNTs:Pt and the Pt foil after the background (indicated by the dashed line) has been subtracted.

platinum ions were converted into their reduced metallic form during the Pt-NP coating process, which increased the number of Pt–Pt bonds and produced an fcc arrangement. This finding indicates that the Pt atoms serve as natural nucleation sites on the surface of N-CNTs and should thereby increase the catalytic activity of Pt–N-CNT nanocomposites.[54] Charge transfer at the interface of the Pt NPs coated onto the N-CNTs is likely. Pt–C and Pt–N are most likely formed when electrons are transferred from Pt 5d to C and N $2p_\pi$ states; this phenomenon is consistent with the weakening of the π^* features at the C and N K-edges and the increase in the intensity of the WL associated with the Pt 5d holes in the Pt L_3-edge spectrum. Moreover, in the post-WL region, the oscillations of features B–D in the N-CNTs:Pt spectra were slightly smaller than those in the spectra of Pt foil because Pt nanoparticles (with a larger surface-to-volume ratio and a lack of long-range order) exhibit greater structural disorder. Fig. 3(b) and the inset show Fourier-transform (FT) spectra and their corresponding EXAFS oscillation $k^2\chi(k)$ at the Pt L_3-edges of N-CNTs:Pt and the Pt foil, respectively. As revealed in the FT spectra, the local atomic structure of the Pt NPs in N-CNTs:Pt closely resembles that of the fcc Pt foil and is also consistent with those of Pt NPs on Pt-CNT and Pt–C_{60} nanocomposites.[55] No significant differences between the local structures of the Pt NPs and the Pt film were observed, which indicates that the Pt NPs deposited onto the N-CNTs are highly stable. However, the amplitude in the FT spectrum of the N-CNTs:Pt, as presented in Fig. 3(b), is clearly much smaller than that of the Pt foil, and the peak maximum shifted to a slightly lower value (as indicated by the dashed lines). As previously stated, this result is primarily caused by the greater structural disorder and by the smaller Pt surface coordination numbers in Pt NPs compared to those in the Pt foil because Pt atoms are bonded with the C and N atoms, thereby forming Pt–C and Pt–N bonds when Pt NPs are deposited onto the N-CNTs. The shortening of the main radical distance in the FT spectrum, as presented in Fig. 3(b), can be explained by the fact that the atomic radius of Pt is 1.83 Å, whereas those of C and N, at 0.91 and 0.75 Å, respectively, are much smaller.[56] The shortening of the main radical distance also indicates the formation of interfacial Pt–C and Pt–N bonds in the N-CNTs:Pt.[48]

Previously theoretical studies related to the interaction of Pt atoms with graphene-like structures have been reported.[57–60] Here, we used DFT calculations to understand the experimental observations. Structural models, where a Pt atom is bound to a $C_{100}H_{20}$, substitutional-N-doped (sN-doped) $C_{94}N_6H_{20}$ or pyridine-like N-doped (PyN-doped) $C_{92}N_6H_{20}$ (10,0) CNT clusters were chosen. The atomic positions of these structural models were optimized, as shown in Fig. 4(a)–(f). The geometric optimizations were performed at the B3LYP/6-31G* DFT level using the Gaussian 03 software package.[36] In these structural models, the dangling bonds are terminated by H atoms to render surface atoms to be bulk-like. In this study, the cluster models without adsorbed Pt atoms were first optimized; in these models, the substitutional N atoms are homogeneously distributed around the sN-doped cluster (ESI Fig. S1†). However, each pyridine-like N site is composed of a vacancy surrounded by three N atoms.[23,61] The optimized atomic arrangements are presented in

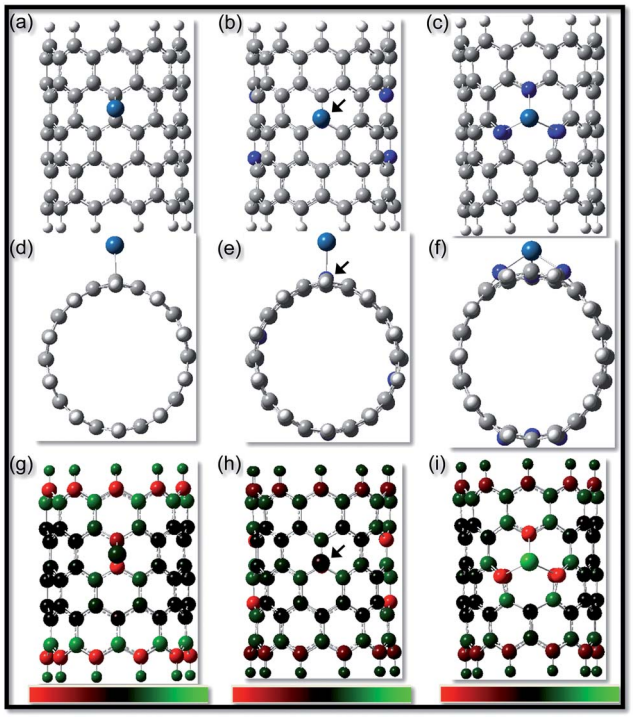

Fig. 4 Optimized geometries of the Pt adatom bound to various CNT clusters. (a) Substitutional-N-doped (b) and pyridine-like N-doped (c) (10,0) CNT clusters. Grey, blue, white, and cyan spheres represent C, N, H, and Pt atoms, respectively. Substitutional N atoms are homogeneously distributed around the nanotube, and each pyridine-like N site is composed of a vacancy that is surrounded by three N atoms. In the two N-doped cases, the Pt adatom remains at the N sites because of the greater binding energies. The arrows in the figure of the substitutional-N-doped CNT clusters indicate the presence of a single N atom beneath the Pt adatom. (d)–(f) show the corresponding cross-sectional views of the previous three cases. Changes in cross-sectional shape are caused by variation in localized N bonding configurations, which distort the nanotube differently (ESI Fig. S1†). (g)–(i) show the corresponding charge density plots for the three previously discussed CNT clusters. The colored bars at the bottom represent the charge, from most negative (red, left) to most positive (green, right); N atoms in the latter two cases all exhibit high negative charges.

ESI Fig. S1.† After the geometries were optimized, a Pt atom was placed on the nanotube surface in each case. The Pt atom remained at the bridge site between two C atoms on the axis of the tube (Fig. 4(a) and (d)). The binding energy was approximately 2.3 eV, and the effective charge of the Pt atom was 0.05. In the sN-doped cluster, the Pt atom was shifted to the top of the substitutional N atom (Fig. 4(b) and (e)). The arrows in the figure of the sN-doped case indicate that an N atom is located beneath the Pt atom. The binding energy of the Pt adatom at the substitutional N site increased drastically to 19.91 eV, which is approximately nine times greater than the binding energy of the Pt adatom on the undoped surface. The effective charge of this Pt adatom at the N site was −0.08, which indicates that the substitutional N with an electron lone pair acts as a donor.[23] The Pt adatom also remained on top of the pyridine-like N site and had a slightly increased binding energy (Fig. 4(c) and (f)). The small increase in the binding energy is attributable to the complex bonding hybridization between orbitals of the Pt adatom and the three N atoms at the pyridine-like site. The Pt–Pt interactions are essential for achieving a further understanding of our system. Actually, A. Maiti and A. Ricca already investigated the metal–undoped nanotube interactions and discussed the binding energies and the wetting properties in their early paper.[62] Their conclusions strongly indicate that the Pt–Pt interactions are very strong compared to Pt–support interactions. Thus, we hypothesize that the binding of the first Pt atom to the tube surface is so critical that the subsequent Pt atoms will attach to the first Pt atom rather than adsorb onto a C-site due to the strong Pt–Pt interactions. As shown in Fig. 1 of our manuscript, the TEM image, which shows uniformly distributed Pt nanoparticles on a single N-doped tube, supports our hypothesis. In contrast, strong Pt–support interactions would lead to the formation of a thin film instead of high-density nanoparticles. Our observations *via* electron microscopy do not indicate the formation of a thin film, although thin-film formation is known to occur for other metals, such as Ti, on nanotubes.[63] The increase in binding energy is consistent with the shift of the edge of the C and N K-edge spectra and the formation of the Pt–C and Pt–N bonds. Because the charge distribution in the DFT calculation may reflect the formation of N-CNTs:Pt, these calculation results may be further related to the shifts in the C and N K-edge XANES spectra.

Conclusions

In conclusion, the atomic-scale N-dopant structures on the CNT surfaces serve as natural nucleation sites for Pt NPs. A combination of experimental measurements and DFT calculations provide a better understanding of the atomic structures of N-CNTs:Pt. Self-organized Pt-NPs on N-doped CNTs are uniformly distributed because of the high binding energies of the Pt adatoms at the defect sites on the surface. The π^* feature is found to be suppressed, and the edge shifts to higher energy at both the C and N K-edges, which indicates that charge transfer most likely occurs at the surface/interface of N-CNTs:Pt during the nucleation process and the formation of the Pt–C and Pt–N bonds.

Acknowledgements

We gratefully thank the National Science Council (NSC 99-2119-M032-004-MY3) and the Ministry of Education in Taiwan for financial support as well as the National Center for High-performance Computing for computer time and facilities. S.C.R. is grateful to NRF South Africa for financial support.

References

1 M. Trau, S. Sankaran, D. A. Saville and I. S. Aksay, *Nature*, 1995, **374**, 437–439.
2 C. B. Murray, C. R. Kagan and M. G. Bawendi, *Science*, 1995, **270**, 1335–1338.
3 A. P. Alivisatos, K. P. Johnsson, X. Peng, T. E. Wilson, C. J. Loweth, M. P. Bruchezjand and P. G. Schultz, *Nature*, 1996, **382**, 609–611.

4 K. Bromann, C. Félix, H. Brune, W. Harbich, R. Monot, J. Buttet and K. Kern, *Science*, 1996, **274**, 956–958.
5 P. Jensen, *Rev. Mod. Phys.*, 1999, **71**, 1695–1735.
6 S. Sun, C. B. Murray, D. Weller, L. Folks and A. Moser, *Science*, 2000, **287**, 1989–1992.
7 F. Goettmann, A. Moores, C. Boissiere, P. L. Floch and C. Sanchez, *Small*, 2005, **6**, 636–639.
8 H. J. Yen, S. H. Hsu and C. L. Tsai, *Small*, 2009, **13**, 1553–1561.
9 D. R. Rolison, *Chem. Rev.*, 1990, **90**, 867–878.
10 Z. Xu, F.-S. Xiao, S. K. Purnell, O. Alexeev, S. Kawi, S. E. Deutsch and B. C. Gates, *Nature*, 1994, **372**, 346–348.
11 J. M. Planeix, N. Coustel, B. Coq, V. Brotons, P. S. Kumbhar, R. Dutartre, P. Geneste, P. Bernier and P. M. Ajayan, *J. Am. Chem. Soc.*, 1994, **116**, 7935–7936.
12 G. Che, B. B. Lakshimi, E. R. Fisher and C. R. Martin, *Nature*, 1998, **393**, 346–349.
13 S. H. Joo, S. J. Choi, I. Oh, J. Kwak, Z. Liu, O. Terasaki and R. Ryoo, *Nature*, 2001, **412**, 169–172.
14 M. S. Chen and D. W. Goodman, *Science*, 2004, **306**, 252–255.
15 K. J. Lee, S. H. Min and J. Jang, *Small*, 2010, **21**, 2378–2382.
16 C. L. Sun, H. H. Lee, J. M. Yang and C. C. Wu, *Biosens. Bioelectron.*, 2011, **26**, 3450–3455.
17 C. Bock, C. Paquet, M. Couillard, G. A. Botton and B. R. MacDougall, *J. Am. Chem. Soc.*, 2004, **126**, 8028–8037.
18 B. J. Hwang, L. S. Sarma, J. M. Chen, C. H. Chen, S. C. Shih, G. R. Wang, D. G. Liu, J. F. Lee and M. T. Tang, *J. Am. Chem. Soc.*, 2005, **127**, 11140–11145.
19 J. Chen, Y. Xiong, Y. Yin and Y. Xia, *Small*, 2006, **2**, 1340–1343.
20 C. Y. Chu, C. T. Tsai and C. L. Sun, *Int. J. Hydrogen Energy*, 2012, **37**, 13880–13886.
21 C. Wang, M. Waje, X. Wang, J. M. Tang, R. C. Haddon and Y. Yan, *Nano Lett.*, 2004, **4**, 345–348.
22 D. Jana, C. L. Sun, L. C. Chen and K. H. Chen, *Prog. Mater. Sci.*, 2013, **58**, 565–635.
23 C. L. Sun, H. W. Wang, M. Hayashi, L. C. Chen and K. H. Chen, *J. Am. Chem. Soc.*, 2006, **128**, 8368–8369.
24 S. A. Stevenson, J. A. Dumesic, R. T. K. Baker and E. Ruckenstein, *Metal–support interactions in catalysis, sintering and redispersion*, Van Norstrand Reinhold, New York, 1987.
25 S. Ye, A. K. Vijh and L. H. Dao, *J. Electrochem. Soc.*, 1997, **144**, 90–95.
26 W. Kohn and L. J. Sham, *Phys. Rev.*, 1965, **140**, A1133–A1138.
27 R. G. Parr and W. Yang, *Density-functional theory of atoms and molecules*, Oxford Scientific Publications, Oxford University Press, Oxford, 1989.
28 B. M. Klein, *Nature*, 1999, **399**, 108–109.
29 C. L. Sun, L. C. Chen, M. C. Su, L. S. Hong, O. Chyan, C. Y. Hsu, K. H. Chen, T. F. Chang and L. Chang, *Chem. Mater.*, 2005, **17**, 3749–3753.
30 C. L. Sun, Y. K. Hsu, Y. G. Lin, K. H. Chen, C. Bock, B. MacDougall, X. Wu and L. C. Chen, *J. Electrochem. Soc.*, 2009, **156**(10), B1249–B1252.
31 C. Liu, C. C. Wang, C. C. Kei, Y. C. Hsueh and T. P. Perng, *Small*, 2009, **5**, 1535–1538.
32 L. Dai, D. W. Chang, J. B. Baek and W. Lu, *Small*, 2012, **8**, 1130–1166.
33 S. Sun, G. Zhang, Y. Zhong, H. Liu, R. Li, X. Zhou and X. Sun, *Chem. Commun.*, 2009, 7048–7050.
34 J. Yang, J. Wang, X. Li, D. Wang, J. Liu, G. Liang, M. Gauthier, Y. Li, D. Geng, R. Li and X. Sun, *J. Mater. Chem.*, 2012, **22**, 7537–7543.
35 X. Li, J. Liu, Y. Zhang, Y. Li, H. Liu, X. Meng, J. Yang, D. Geng, D. Wang, R. Li and X. Sun, *J. Power Sources*, 2012, **197**, 238–245.
36 M. J. Frisch, *et al.*, *GAUSSIAN 03*, Gaussian, Inc., Wallingford CT, 2004, see reference S1.†
37 W.-Q. Han, K.-R. Philipp, T. Seeger, F. Ernst, M. Rühle, N. Grobert, W.-K. Hsu, B.-H. Chang, Y.-Q. Zhu, H. W. Kroto, D. R. M. Walton, M. Terrones and H. Terrones, *Appl. Phys. Lett.*, 2000, **77**, 1807–1809.
38 S. C. Ray, C. W. Pao, J. W. Chiou, H. M. Tsai, J. C. Jan, W. F. Pong, R. McCann, S. S. Roy, P. Papakonstantinou and J. A. McLaughlin, *J. Appl. Phys.*, 2005, **98**, 033708–033711.
39 S. C. Ray, C. W. Pao, H. M. Tsai, J. W. Chiou, W. F. Pong, C. W. Chen, M.-H. Tsai, P. Papakonstantinou, L. C. Chen, K. H. Chen and W. G. Graham, *Appl. Phys. Lett.*, 2007, **90**, 192107.
40 J. G. Zhou, J. Wang, C. L. Sun, J. M. Maley, R. Sammynaiken, T. K. Sham and W. F. Pong, *J. Mater. Chem.*, 2011, **21**, 14622–14630.
41 J. W. Chiou, S. C. Ray, S. I. Peng, C. H. Chuang, B. Y. Wang, H. M. Tsai, C. W. Pao, H.-J. Lin, Y. C. Shao, Y. F. Wang, S. C. Chen, W. F. Pong, Y. C. Yeh, C. W. Chen, L.-C. Chen, K.-H. Chen, M.-H. Tsai, A. Kumar, A. Ganguly, P. Papakonstantinou, H. Yamane, N. Kosugi, T. Regier, L. Liu and T. K. Sham, *J. Phys. Chem. C*, 2012, **116**, 16251–16258.
42 K. Suenaga, C. Colliex and S. Iijima, *Appl. Phys. Lett.*, 2001, **78**, 70–72.
43 E. Frackowiak, G. Lota, K. Lota and F. Béguin, *AIP Conf. Proc.*, 2004, **723**, 532–535.
44 H. C. Choi, S. Y. Bae, W.-S. Jang, J. Park, H. J. Song, H.-J. Shin, H. Jung and J.-P. Ahn, *J. Phys. Chem. B*, 2005, **109**, 1683–1688.
45 S. H. Lim, H. I. Elim, X. Y. Gao, A. T. S. Wee, W. Ji, J. Y. Lee and J. Lin, *Phys. Rev. B: Condens. Matter Mater. Phys.*, 2006, **73**, 045402.
46 J. M. Ripalda, E. Román, N. Díaz, L. Galán, I. Montero and G. Comelli, *Phys. Rev. B: Condens. Matter Mater. Phys.*, 1999, **60**, 3705–3707.
47 S. Bhattacharyya, M. Lubbe and F. Richter, *J. Appl. Phys.*, 2000, **88**, 5043–5049.
48 Y. Zhang, M. L. Toebes, A. van der Eerden, W. E. O'Grady, K. P. de Jong and D. C. Koningsberger, *J. Phys. Chem. B*, 2004, **108**, 18509–18519.
49 I. Robel, G. Girishkumar, B. A. Bunker, P. V. Kamat and K. Vinodgopal, *Appl. Phys. Lett.*, 2006, **88**, 073113.
50 J. Zhou, X. Zhou, X. Sun, R. Li, M. Murphy, Z. Ding, X. Sun and T.-K. Sham, *Chem. Phys. Lett.*, 2007, **437**, 229–232.
51 L. Liu, M. Murphy, J. Y. P. Ko and T. K. Sham, *J. Phys.: Conf. Ser.*, 2009, **190**, 012133.

52 R. M. van der Veen, J. J. Kas, C. J. Milne, V.-T. Pham, A. El Nahhas, F. A. Lima, D. A. Vithanage, J. J. Rehr, R. Abela and M. Chergui, *Phys. Chem. Chem. Phys.*, 2010, **12**, 5551–5561.
53 S. Adora, Y. Soldo-Olivier, R. Faure, R. Durand, E. Dartyge and F. Baudelet, *J. Phys. Chem. B*, 2001, **105**, 10489–10495.
54 J. W. Chiou, S. C. Ray, H. M. Tsai, C. W. Pao, F. Z. Chien, W. F. Pong, C. H. Tseng, J. J. Wu, M.-H. Tsai, C.-H. Chen, H. J. Lin, J. F. Lee and J.-H. Guo, *J. Phys. Chem. C*, 2011, **115**, 2650–2655.
55 I. Robel, G. Girishkumar, B. A. Bunker, P. V. Kamat and K. Vinodgopal, *Appl. Phys. Lett.*, 2006, **88**, 073113.
56 *Table of periodic properties of the elements*, Sargent-Welch Scientific Company, Skokie, Illinois, 1980.
57 O. Okamoto, *Chem. Phys. Lett.*, 2006, **420**, 382.
58 M. Zhou, A. Zhang, Z. Dai, C. Zhang and Y. P. Feng, *J. Chem. Phys.*, 2010, **132**, 194704.
59 A. Pulido, M. Boronat and A. Corma, *New J. Chem.*, 2011, **35**, 2153.
60 O. U. Akturk and M. Tomak, *Phys. Rev. B: Condens. Matter Mater. Phys.*, 2009, **80**, 085417.
61 R. Czerw, M. Terrones, J.-C. Charlier, X. Blase, B. Foley, R. Kamalaka ran, N. Grobert, H. Terrones, D. Tekleab, P. M. Ajayan, W. Blau, M. Rühle and D. L. Carroll, *Nano Lett.*, 2001, **1**, 457–460.
62 A. Maiti and A. Ricca, *Chem. Phys. Lett.*, 2004, **395**, 7.
63 Y. Zhang and H. Dai, *Appl. Phys. Lett.*, 2000, **77**, 3015.